united nations
educational, scientific
and cultural
organization

international atomic
energy agency

the
abdus salam
international centre for theoretical physics

SMR 1521/23

AUTUMN COLLEGE ON PLASMA PHYSICS

13 October - 7 November 2003

Solitary Structures in Relativistic Plasmas

F. Pegoraro

Universita' di Pisa, Dip. di Fisica & INFM
Pisa, Italy

Autumn College on Plasma Physics
Trieste, 2003

Solitary structures in relativistic plasmas

F. Pegoraro

Dipartimento di Fisica Univ. di Pisa and I.N.F.M,
56124 Pisa, Italy

1 Solitons

Solitons are nonlinear structures which arise due to the interplay of nonlinear and dispersion effects.

Solitons have been known for a long time as a special kind of "waves" that occur in media where *nolinearity* (the dependence of the propagation velocity on the wave amplitude) and *dispersion* (the dependence of the propagation velocity on the wave frequency) play equally important roles.

In these media small amplitude waves evolve in the form of wave packets that spread as they propagate, while finite amplitude waves can develop into coherently propagating structures due to their nonlinear self-interaction.

The physics of solitons in different nonlinear media is an open and fast evolving field and their intriguing properties have lead scientists to create new fields in physics and in mathematics: indeed even if solitons were investigated intensively starting from the 60's, up to now very few results are known about three-dimensional solitary waves.

See e.g., :
http://www.ma.hw.ac.uk/solitons/
and more specifically
http://www.ile.osaka-u.ac.jp/research/TSI/Timur/soliton/
(from where some of the figures used are taken)

1.1 Relativistic plasma solitons

In a plasma interacting with an ultra-high intensity electromagnetic (e.m.) wave, wave dispersion appears due to finite electron inertia while nonlinearity is due to the relativistic dependence of the electron mass on its energy and to the electron density redistribution under the ponderomotive pressure of the high intensity e.m. fields.

The interplay of the relativistic nonlinearity and of the plasma dispersion results in the appearance of different types of coherent nonlinear structures such as self-focusing channels that guide the laser pulse and relativistic electron vortices associated with quasistatic magnetic fields (see e.g. the review given in Ref. [1]).

1.2 Investigation strategies

These nonlinear structures are clearly seen, and in some cases were indeed discovered for the first time, in computer simulations and later in laboratory experiments.

When investigating these nonlinear effects, one has to account for the fact that only low-dimensional models can be solved analytically because the complexity of the interaction between the e.m. wave and the plasma, due to the high dimensionality of the problem, to the lack of symmetry and to the importance of nonlinear and kinetic effects, makes analytical methods unable to provide a detailed description.

On the other hand, powerful methods for investigating the laser-plasma interaction have become available through the advent of modern supercomputers and to the developments of applied mathematics.

Supercomputers can now perform fully three-dimensional simulations of the interaction of high intensity laser pulses with plasmas which allow us to obtain detailed information about the nonlinear structures that are generated by a strong e.m. field.

2 Subcycle solitons

Relativistic plasma solitons are self-trapped and spatially confined nonlinear e.m. waves that propagate in a plasma without diffraction spreading.

They are formed during the interaction of ultra-intense laser pulses with plasmas and are generated as the result of the frequency downshift due to pulse energy depletion [2].

Self-trapping appears because a high amplitude e.m. wave modifies the local refractive index through the relativistic increase of the electron mass and the redistribution of the electron density under the pondermotive pressure of the radiation.

Different relativistic soliton branches have been discussed in the literature: of special interest here is the branch corresponding to non-propagating solitons, which are called "subcycle solitons" because the e.m. fields inside them have a spatial structure that corresponds to a single half-cycle oscillation.

Numerical simulations and experimental results indicate that a sizable fraction of the laser pulse energy is transformed into subcycle soliton energy during the laser pulse interaction with the plasma.

The ion dynamics affects these soliton branches differently: on times long on the electron dynamical times when ions can no longer be assumed to remain at rest, subcycle solitons evolve into quasineutral slowly expanding "post- soliton" structures characterized by a slowly growing hole in the plasma density.

The quasistationary nature of the charge-separation electric field associated to these post-soliton structures makes their experimental detection possible.

2.1 1-D analytical results

We shall first recall some analytical results that have been recently discussed in the case of 1-D relativistic solitons in plasmas.

In 2-D and 3-D configurations no such exact solutions are available due to the complexity of the nonlinear plasma response to multi-dimensional e.m. fields and, in 3-D, of the fields' topological structure.

We start by introducing the well known equations (see e.g., [3]) that describe finite amplitude circularly polarized waves in a cold collisionless unbounded relativistic plasma with immobile ions.

In the Coulomb gauge div $\mathbf{A} = 0$, Maxwell's equations give

$$\Delta\mathbf{A} - \frac{1}{c^2}\partial_{\rm tt}\mathbf{A} - \frac{1}{c}\nabla\partial_{\rm t}\varphi - \frac{4\pi e n_e}{m_e c^2 \gamma}(\mathbf{P} + \frac{e}{c}\mathbf{A}) = 0, \quad (1)$$

$$n_e = n_i(x) + \frac{1}{4\pi e}\Delta\varphi, \quad (2)$$

where $\mathbf{P} \equiv \mathbf{p} - e\mathbf{A}/c$ is the canonical electron momentum, the relativistic Lorentz factor is

$$\gamma = \left[1 + (\mathbf{P} + e\mathbf{A}/c)^2/(m_e c^2)\right]^{1/2}$$

and $n_i(x)$ is the density of the fixed ion background.

We model the electron response using the hydrodynamic equations of a cold electron fluid.

Then the electron momentum equation can be put in the form

$$\partial_{\rm t}\mathbf{P} = \nabla(e\varphi - m_e c^2\gamma) + \frac{1}{\gamma}(\mathbf{P} + \frac{e}{c}\mathbf{A}) \times (\nabla\times\mathbf{P}), \quad (3)$$

while the continuity equation is automatically implied by Eqs.(1,2).

We consider 1-D solutions where $\partial_{\rm y} = \partial_{\rm z} = 0$.

Then the Coulomb gauge gives $A_x = 0$ and we can choose initial conditions such that the conserved y and z components of the canonical momentum vanish ($P_{\rm y} = P_{\rm z} = 0$).

Assuming the e.m. wave to be circularly polarized, we introduce the new independent variables $X = x - v_s t$ and $\tau = t$ and look for solutions of the form:

$$\mathbf{A}_\perp = A_{\rm y} + iA_{\rm z} = A(X)\exp[i\omega((1-\beta_s^2)\tau - v_s X/c^2)], \tag{4}$$

$$p_{||}/m_e c = \beta_s b(X),$$

so that $|\mathbf{A}_\perp|$ is independent of τ.

Inserting Eq.(4) into Eqs.(1-3) and assuming the ion density to be homogeneous, we obtain the following system of coupled ordinary differential equations

$$\left(\gamma - \beta_s^2 b\right)'' = \frac{\omega_{pe}^2 b}{(\gamma - b)c^2}, \tag{5}$$

$$a'' + \frac{\omega^2}{c^2}a = \frac{\omega_{pe}^2 \gamma_s^2}{(\gamma - b)c^2}a,$$

where $\gamma = (1 + a^2 + \beta_s^2 b^2)^{1/2}$, $\gamma_s = (1-\beta_s^2)^{-1/2}$, $\beta_s = v_s/c$, $a = eA/m_e c^2$, and a prime denotes a differentiation with respect to the variable X.

This system of equations corresponds to the Hamiltonian motion of a "particle" in a two dimensional potential field [4, 5].

Setting $b = 0$ in Eqs.(5) we obtain a purely transverse nonlinear e.m. wave with $A(X)$ constant and frequency ω given by [6]

$$\omega = \omega_{pe}\gamma_s/(1+a^2)^{1/4}, \tag{6}$$

which is equivalent to $\omega^2 = k^2c^2 + \omega_{pe}^2/(1+a^2)^{1/2}$ with wavenumber $k = v_s\omega/c^2$.

In this case v_s is the group velocity of the wave and the wave phase velocity is $\omega/k = c^2/v_s$.

Localized solutions are obtained by imposing the boundary conditions $a(\infty) = b(\infty) = 0$ [7].

In this case the system of Eqs.(5) describes one-dimensional relativistic e.m. solitons propagating through a cold collisionless plasma. For a small but finite amplitude, an isolated "envelope soliton " solution [8] is described by the well known hyperbolic secant expression:

$$a = \frac{2[1-(\omega/\omega_{pe}\gamma_s)^2]^{1/2}\exp[i\omega((1-\beta_s^2)\tau - v_sX/c^2)]}{\cosh\left[k_p^2X\left(1-(\omega/\omega_{pe}\gamma_s)^2\right)^{1/2}\right]}, \tag{7}$$

with frequency $\omega \approx \omega_{pe}\gamma_s(1 - a_m^2/8)$, and amplitude $a_m = a(0,0)$.

An exact solution [9, 10] can be found in the limit of a soliton with zero propagation velocity. In the case $\beta_s = 0$, b vanishes and Eqs.(5) reduce to

$$a'' + k_p^2[(\omega/\omega_{pe})^2 - (1 + k_p^2\gamma'')/\gamma]a = 0\,, \qquad (8)$$

from which we obtain a soliton solution of the form

$$a(X,\tau) = \frac{2[1-(\omega/\omega_{pe})^2]^{1/2}\ \cosh\left[k_p^2 X\left(1-(\omega/\omega_{pe})^2\right)^{1/2}\right]\exp(i\omega\tau)}{\cosh^2\left[k_p^2 X\left(1-(\omega/\omega_{pe})^2\right)^{1/2}\right] + 1 - (\omega/\omega_{pe})^2}\ , \qquad (9)$$

where $k_p = \omega_{pe}/c$. The soliton frequency ω depends on the soliton amplitude $a_{\rm m}$ as

$$a_{\rm m} = 2\omega_{pe}(\omega_{pe}^2 - \omega^2)^{1/2}/\omega^2\ . \qquad (10)$$

This single-hump soliton solution is stable provided the electron density inside it does not vanish.

This imposes the constraints $a_{\rm m} < \sqrt{3}$ and

$$1 > (\omega/\omega_{pe}) > \sqrt{2/3}. \qquad (11)$$

See figs 01- 02

The solution given by Eq.(9) has been extended in Ref. [11] to the case of a soliton in a uniform magnetised plasma. In this case, the maximum allowed amplitude corresponding to the zero electron density depends on the magnetic field intensity and on its sign.

For negative values of Ω/ω, with $\Omega = eB/m_e c$, solitons exist with amplitudes appreciably larger and frequencies lower than in the unmagnetised case.

The effect on the ion motion on the propagating envelope (multi-humped) solitons has been investigated in detail in Ref. [12] where it is shown that no solution can be found for propagation velocities v_s smaller than a critical value $v_{s,cr}$.

This implies that the non propagating solution given in Eq. (9) is not continuously connected to those with $v_s \neq 0$ and that its structure will change on the ion dynamical time.

The relativistic hydrodynamic equations for a hot multicomponent plasma have been derived in Ref. [13], by assuming an adiabatic closure leading to the entropy conservation for each species. In this framework , 1-D relativistic electromagnetic solitons in electron-positron plasmas have been studied in Refs. [13, 14].

In Ref. [15], an isothermal hydrodynamic model has been formulated starting from the exact solution of the relativistic Vlasov equation for circularly-polarized e.m. radiation in a 1-D multi-component plasma.

Relativistic solitons in an electron-positron plasmas [15] and in a quasi-neutral electron-ion plasma [16] have been investigated in this context. In all cases, equilibria with extremely high field intensities in strongly overdense plasmas have been obtained.

2.2 Analytical models and numerical results for higher-dimension relativistic subcycle solitons

In two and three dimensions exact solutions for relativistic e.m. solitons of the type described above are not available and it is worth noting that the nonlinear wave evolution in 3-D regimes differs drastically from the 1-D and 2-D cases, as shown, e.g., by the problem of wave collapse [17].

Numerical simulations both in 2-D and in 3-D [18, 19] indicate that long-lasting coherent soliton-like structures, where e.m. energy from the laser pulse is self trapped, do occur. Indeed, relativistic solitons are now routinely observed in two dimensional simulations [20, 21].

See Figs 03 -04

The solitons found in these simulations consist of slowly or non propagating electron density cavities inside which an e.m. field is trapped and oscillates coherently with a frequency below the unperturbed plasma frequency and a spatial structure corresponding to half a cycle.

In the 2-D case, the analogues of Eq.(8) can be obtained in the limit of weak nonlinearity for linearly polarized *s*- and *p*- solitons. In *s*-polarized solitons the z-component of the electric field and the azimuthal component of the magnetic field oscillate in time, while the electron density distribution remains constant.

Assuming for the vector potential a time dependence of the form $a(r)\exp\left[-i(\omega_{\rm pe}-\delta\omega)t\right]$, we find

$$r^{-1}\partial_r r\partial_r a - k_p^2[2\delta\omega/\omega_{\rm pe} - |a|^2]a = 0. \qquad (12)$$

This equation describes localized 2-D solitons with frequency shift $\delta\omega$ and radius r_0 which depend on the soliton amplitude as $\delta\omega \sim a^2$ and $r_0 \sim 1/a$.

This scaling agrees with the dependence of the frequency on the soliton amplitude found above in the case of a planar circularly polarized 1-D soliton.

In p-polarized solitons the electric field is azimuthal and the magnetic field is directed along z and for the amplitude $a_\varphi(r)$ we obtain

$$r^{-1}\partial_r r\partial_r a_\varphi - r^{-2}a_\varphi - k_p^2(2\delta\omega/\omega_{\rm pe} - |a|^2)a_\varphi = 0. \quad (13)$$

The typical form of the s- and p- solitons obtained by numerical integration of Eqs.(12,13) are discussed in [18].

The information provided by these analytical models is found to be in agreement with the results of the numerical simulations of 2-D solitons reported in Refs. [18, 20] and reviewed in Ref. [3].

An example of such 2-D soliton simulations presented in ref. [18] is shown in the figures 03.

Here we briefly recall two important results that have been displayed by these simulations.

First, collisions between two 2-D s-solitons have been observed and shown to lead to the synchronization and eventual merging of two s-solitons, differently from the results presented in Ref. [10] for circularly polarized 1-D solitons, where each soliton maintains its amplitude and propagation speed while their phases change.

This indicates that in 2-D some of the characteristic properties of solitons are not recovered.

Second, in an inhomogeneous plasma the propagation of the sub-cycle solitons is strongly affected by the inhomogeneity of the medium which can be exploited in order to extract and detect the solitons.

A simple model of the soliton motion derived by referring to the propagation of a wave packet in a non-uniform dispersive medium shows that the wave packet is accelerated towards the low density side of the plasma and, if a density channel is formed e.g., by the laser pulse, the soliton oscillates in the transverse direction.

As a result, the soliton moves towards the plasma vacuum interface.

See Fig 05

The trapping of the e.m. energy becomes weaker as the solitons move towards regions of lower density until their local oscillation frequency becomes larger than the ambient plasma frequency when they burst into low frequency e.m. radiation. These radiation bursts might be used in order to detect subcycle solitons.

Three dimensional simulations of laser induced sub-cycle relativistic e.m. solitons have been performed only recently in Ref. [19] using the REMP - Relativistic Electro-Magnetic Particle-mesh code [22] based on the Particle-in-Cell method.

We could expect that, knowing the properties of the various types of two dimensional solitons, one could have easily guessed the topological structure of a three dimensional soliton.

However, in generalizing the 2-D results to a fully 3-D configuration a new problem arises from the vector nature of the fields i.e., from the topological constraints that are encountered when trying to confine the e.m. fields inside a finite 3-D domain.

In view of the difficulty of presenting an complete analytical model of a relativistic 3-D e.m. soliton, we refer explicitly the numerical results obtained in Ref. [19].

The pulse considered in these simulations has a dimensionless amplitude $a = eE_z/(m_e\omega c) = 1$, corresponding to the peak intensity $I = 1.38 \cdot 10^{18}\mathrm{W/cm}^2$ for a $\lambda = 1\mu\mathrm{m}$ laser pulse.

The pulse propagates in a plasma with density $(\omega/\omega_{pe})^2 = 7.7$ along the x-axis and is linearly polarized along z, with a gaussian envelope with FWHM size $8\lambda \times 5\lambda \times 5\lambda$. Its focal plane is placed in front of the plasma slab at the distance of 3λ. Ions and electrons have the same absolute charge, and the mass ratio is $m_i/m_e = 1836$. The length of the plasma slab is 13λ.

These simulations are computationally expensive: the simulation box has $660 \times 400 \times 400$ grid points with a mesh size of 0.05λ. The total number of quasiparticles is $426 \cdot 10^6$.

The boundary conditions are periodic along the y- and z-axes and absorbing along the x-axis for both the EM radiation and the quasiparticles.

The simulations were performed on 16 processors of the NEC SX-5 vector supercomputer in Cybermedia Center, Osaka University.

The soliton consists of oscillating electrostatic and electromagnetic fields confined in a prolate cavity in the electron density. The cavity size is approximately $2\lambda \times 2\lambda \times 3\lambda$ and is is azimuthally symmetric.

The electric field inside the cavity is so large that the quivering distance of electrons in the z-direction is of the order of the cavity size, which results in pulsations of the cavity.

The soliton has an electrostatic component and an inductive poloidal component, while the magnetic field is toroidal so that its structure resembles the lowest eigenmode of a cavity resonator with a deformable wall.

In the equatorial plane the structure of the 3-D soliton is similar to that of a 2-D s-soliton, while that in the perpendicular planes is similar to a 2-D p-soliton.

The electrostatic and e.m. components are of the same order of magnitude.

The e.m. field trapped in the oscillating cavity pulsates at a frequency Ω_S, smaller than the surrounding unperturbed Langmuir frequency, $\Omega_S \approx 0.87\omega_{pe}$.

The density of cavity walls is $2 - 3n_{cr}$. Therefore the e.m. energy can not be radiated away, and, in addition, the soliton oscillation does not resonate with plasma waves. Ses Figs. 06- 07 -08

3 Subcycle soliton evolution

Besides supporting the analytical results and models on the soliton structure in configurations with different dimensionality, numerical simulations allow us to identify the mechanism of sub-cycle soliton generation and, on longer time scales, to account for the effect of the ion dynamics. As mentioned above, the results obtained in the 1-D limit, which show that no solution corresponding to non-propagating solitons is found when mobile ions are considered, indicate that subcycle solitons are expected to be significantly affected by the ion dynamics.

3.1 Adiabatic pulse energy depletion and soliton generation

The physical mechanism that produces sub-cycle solitons, as seen in the numerical simulations, is different from the standard process where the nonlinear steepening of the wave is counterbalanced by the effect of dispersion.

In the present case the dispersion effects come into play because of the frequency downshift of the laser pulse [2]. Interacting with the underdense plasma the laser pulse loses its energy as it generates electrostatic and magnetostatic wake fields behind it.

Since the frequency of these fields is much lower than the carrier frequency of the laser pulse the laser-plasma interaction can be taken to be adiabatic: thus the ratio between the e.m. energy density and frequency is adiabatically conserved and the decrease of the laser pulse energy is accompanied by the downshift of its carrier frequency.

On the other hand the group velocity of the laser pulse decreases as the carrier frequency is downshifted and the pulse group velocity tends to zero at $\omega \rightarrow \omega_{\rm pe}$ so that the depleted portions of the pulse lag behind and convert their energy into soliton energy with almost zero group velocity.

The effectiveness of this is mechanism can be verified by correlating the location of the soliton formation in the PIC simulations with the pulse depletion length, and is rather general.

Therefore we can expect that relativistic subcycle solitons represent one of the main channels of conversion of the energy of propagating relativistically intense e.m. radiation into trapped radiation and eventually into plasma energy.

3.2 Soliton transformation into slowly expanding post-solitons

The soliton formation time is much shorter than the ion response time so that ions can be assumed to be at rest during this phase.

For times longer than $\sqrt{m_i/m_e}$ oscillation periods of the e.m. fields inside the soliton, the ponderomotive pressure created by these fields starts to dig a hole in the ion density and the parameters of the soliton change.

Although this implies that strictly speaking, subcycle solitons cease to behave as solitons on the ion timescale, numerical simulations [21, 19] show that, independently of the dimensionality of the configuration, a low frequency e.m. wave packet remains in the plasma and is well confined inside a slowly expanding plasma cavity.

In Ref. [21] this nonlinear e.m. wave packet has been defined as a "post-soliton".

We can describe the scenario of the post-soliton formation as follows. In the first phase, for times shorter than the ion dynamical time, the ponderomotive pressure of the e.m. fields inside the soliton is balanced by the force due to the electric field which appears due to charge separation.

The ponderomotive pressure displaces the electrons outwards so that, on ion times, the Coulomb repulsion in the electrically non neutral ion core pushes the ions away.

The typical ion kinetic energy corresponds to the electrostatic potential energy which is of the order of $m_e c^2 a$, with a the dimensionless amplitude of the oscillating e.m. fields inside the soliton. The ion expansion in the radial direction leads to the formation of a hole in the ion density.

This plasma cavity forms a resonator for the trapped e.m. field. As this cavity expands, the amplitude and the frequency of the e.m. field decrease.

Since the radius R of the cavity increases very slowly compared to the period of the e.m. field oscillations we can exploit the adiabatic invariant given by the ratio between the energy and the frequency of the e.m. field $\int \mathbf{E}^2 dV/\omega_s = const.$

As a simple analytical model to describe the e.m. field inside the post-soliton, we can use the well known electric- or magnetic-dipole oscillations inside a spherical resonator where the frequency is proportional to the inverse of the cavity radius R.

Then, from $\int \mathbf{E}^2 dV/\omega_s = const$ we obtain that

$$E^2 \sim R^{-4}.$$

Under the action of the e.m. pressure the walls of the cavity expand.

In the "snow plough" approximation [23] all the mass of the plasma pushed by the e.m. pressure $\langle \mathbf{E}^2 \rangle / 8\pi$ is located inside a thin shell.

The mass inside the shell is equal to the mass M initially contained inside a sphere of the radius R: $M = 4\pi n_0 m_i R^3/3$ where n_0 is the unperturbed plasma density.

Then from Newton second law, with

$$\left\langle \mathbf{E}^2 \right\rangle = \left\langle \mathbf{E}_0^2 \right\rangle (R_0/R)^4$$

where E_0 is the amplitude of the electric field inside the soliton and $R_0 \approx c/\omega_{pe}$ is the soliton radius, we obtain

$$\frac{d}{dt}\left(R^3 \frac{dR}{dt}\right) = \frac{3R_0^4 \left\langle \mathbf{E}_0^2 \right\rangle}{8\pi n_0 m_i R^2}, \tag{14}$$

which gives

$$\frac{R}{R_0} = \left[\frac{(2\tau^2)^{2/3} + (2\tau^2 + t^2 + t\sqrt{4\tau^2 + t^2})^{2/3}}{(2\tau^2)^{1/3}(2\tau^2 + t^2 + t\sqrt{4\tau^2 + t^2})^{1/3}} - 1\right]^{1/2}. \tag{15}$$

The timescale of the cavity expansion is equal to

$$\tau = \sqrt{6\pi R_0^2 n_0 m_i / \langle \mathbf{E}_0^2 \rangle}.$$

Asymptotically, when $t \to \infty$, the post-soliton radius increases as

$$R \approx R_0 (2t/\tau)^{1/3}.$$

the amplitude of the e.m. field and its frequency decrease as $E \sim t^{-2/3}$and $\omega_s \sim t^{-1/3}$ (in the case of a cylindrical cavity, we would find $R \sim t^{2/5}$, for $t \to \infty$).

The 2-D numerical simulations show the formation of a post-soliton and its slow expansion, as shown in Fig.09 which is taken from Ref. [21].

See Fig 09

As mentioned before, in the case of wide laser pulses a cloud of solitary waves is produced in the pulse wake.

At later times this soliton cloud evolves into post-solitons as shown in Fig.09 for an s-polarized pulse with amplitude $a = 1$, width 30λ and length 15λ in an under-dense plasma ($n/n_{cr} = 0.64$) at $t = 70$. In the distribution of the electron and ion densities we see a "necklace" of the post- solitons.

As these post solitons expand, they coalesce into large regular structures (post- soliton bubbles) that continue to grow and remain stable against non spherical (non circular) deformations, as discussed in Ref. [24] where the stabilizing effect of the mass accretion on the onset the Rayleigh-Taylor instability is discussed in 1, 2 and 3 dimensions.

The evolution of a 3-D soliton into a post soliton is also evident in the 3-D simulations presented in Ref. [19].

4 Experimental detection of relativistic solitons

The identification of the nonlinear structures, such as self-focussing channels, current filaments, magnetic vortices and solitons, that are produced by the interaction of high-intensity laser pulse with a plasma, and the investigation of their time evolution represent a difficult experimental challenge. In the case of solitons, a key ingredient in their identification may be represented by the bursts of low frequency radiation that they are expected to emit when they exits an inhomogeneous plasma from the low density side, as mentioned before in the case of 2-D simulations (see the first of Refs. [20]; the occurrence of these bursts

has also been confirmed for 3-D solitons in Ref. [19]). No positive soliton identification based on an unambiguous detection of such bursts is as yet available.

On the contrary, the transformation of the non-propagating sub-cycle solitons into quasi-neutral, long lived, post solitons makes it possible to infer the occurrence of solitons in the plasma, through the deflection of the proton beam in the proton imaging technique [25].

4.1 Post-soliton detection by proton imaging techniques

The first experimental observation of a post-soliton bubble was recently reported in Ref. [26].

The experiment was carried out at the Rutherford Appleton Laboratory employing the VULCAN Nd:glass laser operating in the Chirped Pulse Amplification mode (CPA).

The VULCAN CPA pulse was split in two separate 1 ps, 1 μm, 20 J pulses (CPA_1 and CPA_2) which were focussed onto separate targets in a 10-15 μm FWHM focal spot giving an average intensity of about 10^{19} W/cm^2.

The CPA_1 pulse was used as the main interaction pulse and focused into a preformed plasma (see Fig.10). The plasmas were produced by exploding thin plastic foils

(0.3 μm thick) with two 1 ns, 0.527 μm laser pulses at a total irradiance of about 5×10^{14} W/cm^2.

The delay between plasma formation and interaction was typically 1 ns. The CPA_2 pulse was focussed onto a 3 μm Al foil in order to produce a beam of multi-MeV protons, which were used as a transverse particle probe of the interaction region.

As the proton source is small, the proton probe could be used in a point-projection imaging arrangement with the magnification determined by $1 + Z/Z_s$, where $Z = 2cm$ and $Z_s = 2mm$ are respectively the object-to detector and object-to source distances.

Bubble-like structures in proton images of laser-produced plasmas were interpreted in Ref. [26] as the macroscopic remnants of solitons formed during the interaction with the ultraintense pulse.

The observed structures correspond to localized depletion regions in the cross section of a transverse-propagating proton probe beam. The bubbles appear as the protons are deflected away by the localized electric field at the edges of the cavitated areas.

Proton images of the plasma obtained with $6-7$ MeV protons and recorded, in different shots, at various delays after the interaction are shown in Fig.10: 5-6 bubble-like

structures are clearly visible at the centre of the plasma corresponding to delays of $45ps$ after the CPA_1 interaction. In particular a large structure with radius of approximately $50\mu m$ is seen at the centre of the picture.

In the single particle approximation, which applies when the Debye shielding of the electrons accompanying the probe proton beam occurs on a scalelength bigger than the bubble size, it is possible to find both the size of the bubble and the value of the quasistatic electric field inside from the observed proton image of the bubble.

In the case of protons with $\approx 6\ MeV$ energy the effect of the oscillating electromagnetic field is averaged out during the proton transit time. We take the quasistatic electric field $E_{||}$ inside the post-soliton due to charge separation to be of the order [21] of $E_{||} \approx E_0(R_0/R)^4$ and to be directed normally to its walls and to vanish outside the cavity. Further, we assume that the post-soliton bubble has a spherical shape and that the $E_{||}$ has a linear spatial dependence $E_{||} = E_{||0}(r/R)$.

Then, the transverse momentum gained from $E_{||}$ by a proton crossing with velocity v_z and impact parameter r_0 a bubble of radius R, is given or $r_0 < R$ by $\Delta p_\perp \approx (2eE_{||0}r_0/v_z)\sqrt{1 - r_0^2/R^2}$ fand $\Delta p_\perp = 0$ for $r_0 > R$.

The resulting proton density distribution, see Fig.10,

at the distance Z from the bubble located at a distance $Z_s < Z$ from the point-like proton source is approximately constant inside the radius $r_1 = R(1 + Z/Z_s)$, i.e. inside the geometrical projection of the bubble on the image plane, has a jump at r_1 and tends to infinity at the caustic at r_2.

For relatively small deflections, $r_2 = r_1 + \delta r$ with $\delta r \approx (r_1/2)(eE_{||0}Z_s/m_p v_z^2)^2$. From the structure of the central bubble in Fig.6 we can estimate $\delta r \approx 0.3 r_1$ with $r_1 \approx 530 \mu m$.

For $m_p v_z^2/2 = 6\ MeV$, with $Z = 2cm$ and $Z_s = 2mm$, we obtain $E_{||0} \approx 4 \cdot 10^7\ V/cm$, $R \approx 50\mu$.

5 Conclusions

Analytical and numerical investigations show that in the complex physics of the interaction of high intensity ultrashort laser pulses with plasmas, fundamental physical mechanisms can be identified that form the basic blocks of the nonlinear physics of continuous media such as vortices and solitons. The basic features of the vortex and soliton formation and dynamics have been described.

References

[1] S.V. Bulanov, *et al.*, in "Reviews of Plasma Physics" ed. V.D. Shafranov **22**, 227, Kluwer Academic, Consultants Bureau, New York (2001).

[2] S.V. Bulanov, *et al.*, Plasma Phys. Rep., **21**, 550 (1995)

[3] S.V. Bulanov, *et al.*, Physica D, **152-153**, 682 (2001).

[4] V.A. Kozlov, A*et al.*, Sov. Phys. JETP, **76**, 148 (1979).

[5] P.K. Kaw, *et al.*, Phys. Rev. Lett., **68**, 3172 (1992);

[6] A.I. Akhiezer, R.V. Polovin, Sov. Phys. JETP **30**, 915 (1956).

[7] J.H. Marburger, R.F. Tooper, Phys. Rev. Lett. **35**, 1001 (1975).

[8] N L. Tsintsadze, D.D. Tskhakaya, Sov. Phys. JETP, **45**, 252 (1977);

K. Mima, T. Ohsuga, H. Takabe, *et al.*, Phys. Rev. Lett., **57**, 1421 (1986);

H.H. Kuehl, *et al.*, Phys. Rev., **E 47**, 1249 (1993);

V.I. Berezhiani, S.M. Mahajan, Phys. Rev. Lett., **73** , 1110 (1994);

R.N. Sudan, *et al.*, Phys. Plasmas, **4**, 1489 (1997);

N.L. Tsintsadze, *et al.*, Phys. Rev., **E 58**, 4890 (1998).

[9] T. Kurki-Suonio, *et al.*, Phys. Rev., **A 40**, 3230 (1982).

[10] T.Zh. Esirkepov, *et al.*, JETP Letters, **68**, 36 (1998).

[11] D. Farina, *et al.*, Phys. Rev. E 62, 4146 (2000).

[12] D. Farina, S.V. Bulanov, Phys. Rev. Lett. **86**, 5289 (2001);

D. Farina, S.V. Bulanov, Plasma Phys. Rep. **27**, 641 (2001).

[13] M. Lontano, *et al.*, Phys. Plasmas 8, 5113 (2001).

[14] V.I. Berezhiani, *et al.*, Phys. Rev **E 65**, 047402 (2002).

[15] M. Lontano, *et al.*, Phys. Plasmas **9**, 5113 (2002).

[16] M. Lontano,*et al.*, 1. AIP Conference Proceedings. **634**, 87-98 (2002)

[17] V. E. Zakharov, Sov. Phys. JETP **35**, 908 (1972);
E. A. Kuznetsov, Chaos **6**, 381 (1996).

[18] S.V. Bulanov, T.Zh. Esirkepov, *et al.*, Phys. Rev. Lett., **82**, 3440 (1999).

[19] T.Zh. Esirkepov, *et al.*, Phys. Rev. Lett., **89**, 275002 (2002).

[20] Sentoku, Y. *et al.*, Phys. Rev. Lett., **83**, 3434 (1999);
Mima, K. *et al.*, Phys. Plasmas, **8**, 2349 (2001);

[21] Naumova, N.M. *et al.*, Phys. Rev. Lett., **87**, 185004 (2001).

[22] T. Zh. Esirkepov, Comput. Phys. Comm. **135**, 144 (2001).

[23] Ya.B. Zel'dovich, Yu.P. Raizer, "Physics of Shock Waves and High-Temperature Hydrodynamic Phenomena", (Academic Press, N.Y.: 1967).

[24] S.V. Bulanov, F. Pegoraro, Phys. Rev. **E, 65**, 066405 (2002).

[25] M. Borghesi, *et al.*, Plasma Phys. Control. Fus. **43**, A267 (2001).

[26] M. Borghesi *et al.*, Phys. Rev. Lett., **88**, 135002 (2002).

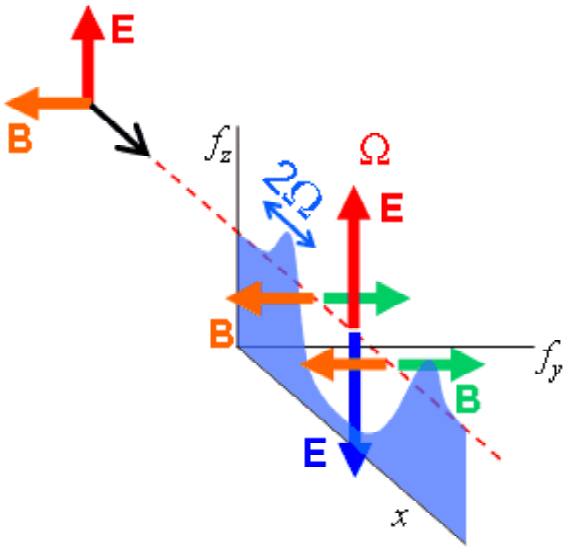

Linearly polarized laser pulse

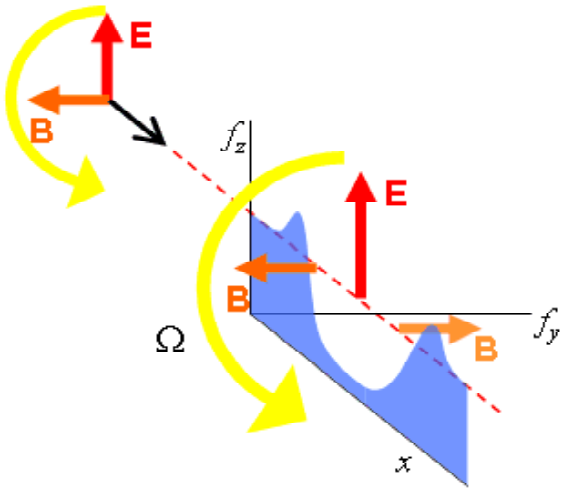

Circularly polarized laser pulse

1 dimensional subcycle soliton solution

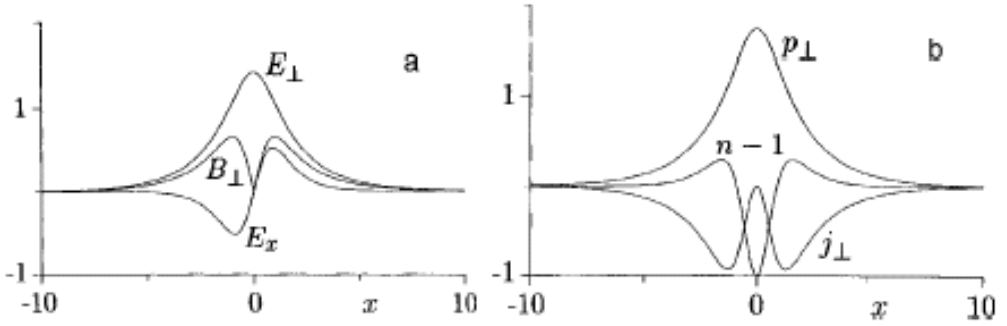

FIG. 1. Electromagnetic fields and the momentum and density of electron fluid in the soliton. a — Fields $E_\perp$, $B_\perp$, E_x. b — Transverse momentum $p_\perp$ and density n of the electron fluid and the transverse current $j_\perp$.

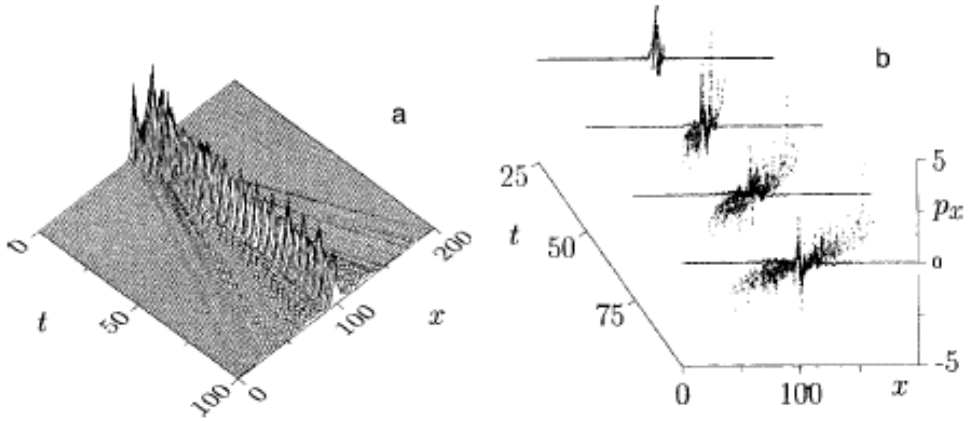

FIG. 3. Breaking of a soliton with overcritical amplitude $A_0=3$ and acceleration of the electrons. a — Evolution of the electron transverse momentum averaged over the cell, $p_\perp$. b — Phase plane (x,p_x) in time.

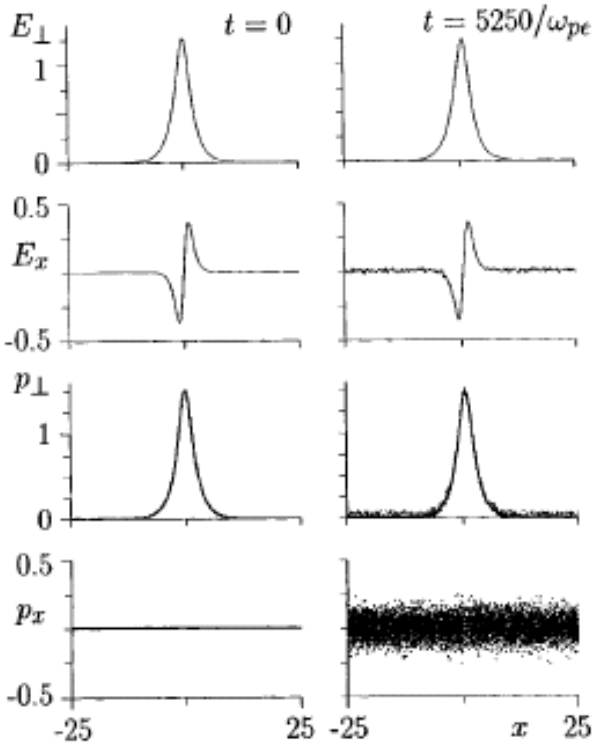

FIG. 2. Stability of a soliton of amplitude $A_0=1.5$, given by (7), (9). The transverse and longitudinal electric fields are shown as functions of time along with the transverse and longitudinal momentum of the electrons. The steady-state electron temperature is $T_e\sim(2-4)\times10^{-3}mc^2$.

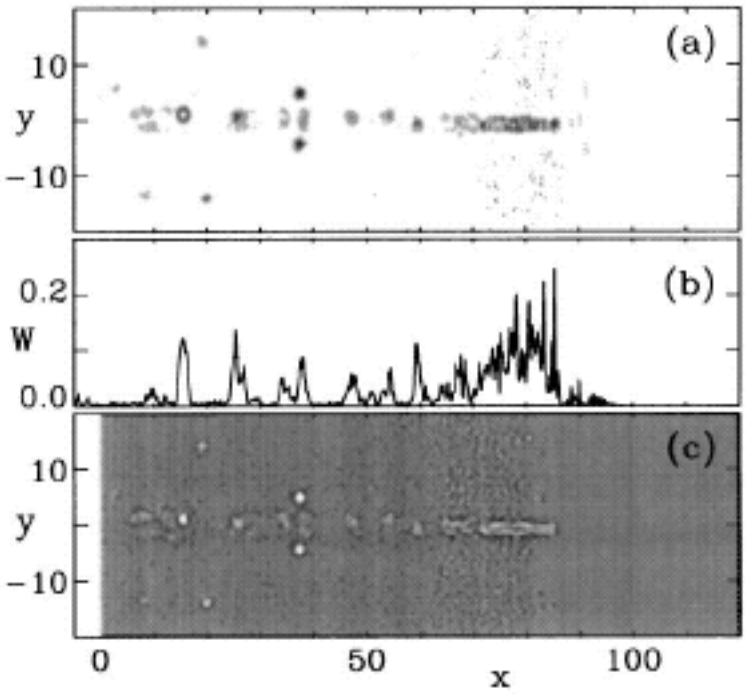

FIG. 1. Solitary waves in the $(x\text{-}y)$ plane behind a pulse with amplitude $a = 3$, width 5λ, and length 10λ in a plasma with $n/n_{cr} = 0.2025$ at $\omega t/2\pi = 120$. (a) Distribution of the square root of the electromagnetic energy density in the $(x\text{-}y)$ plane; (b) electromagnetic energy density on the axis versus x; (c) electron density marking the solitary waves.

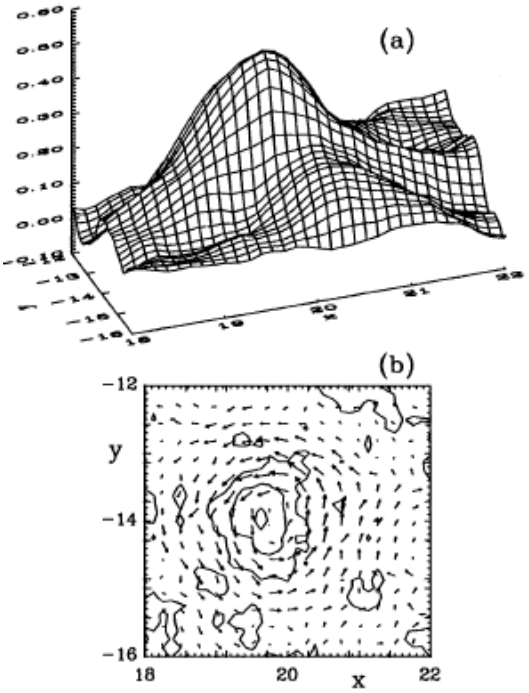

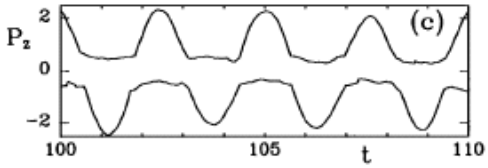

FIG. 4. (a) 2D plot in the $x\text{-}y$ plane of E_z inside the s-polarized solitary wave of Fig. 1(a) at $x \approx 20$, $y \approx -14$ at $\omega t/2\pi = 106$. (b) The corresponding density contours and the vector plot of the magnetic field at $\omega t/2\pi = 105$. (c) Time dependence of the maximum positive and negative values of the momentum along z of the different electrons inside the solitary wave.

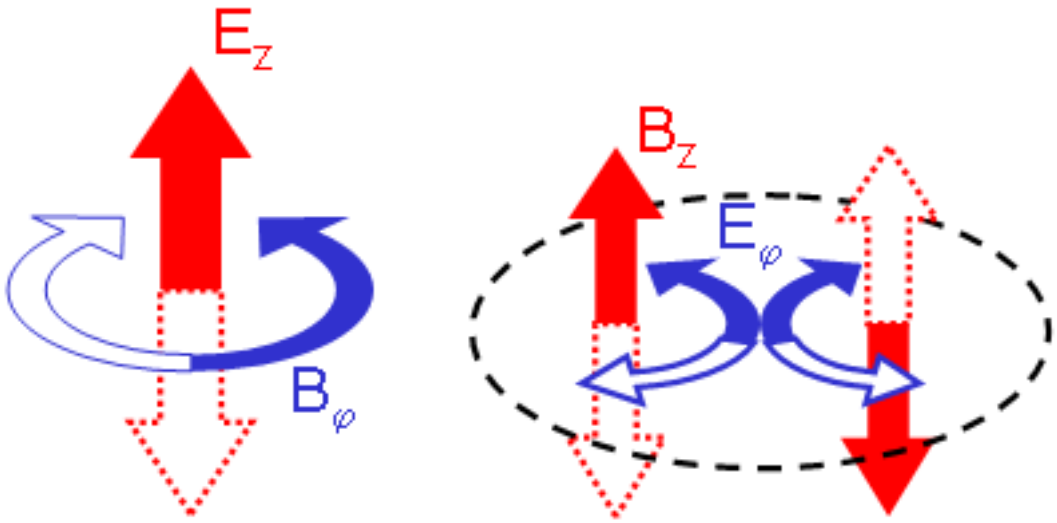

s soliton fields

p soliton fields

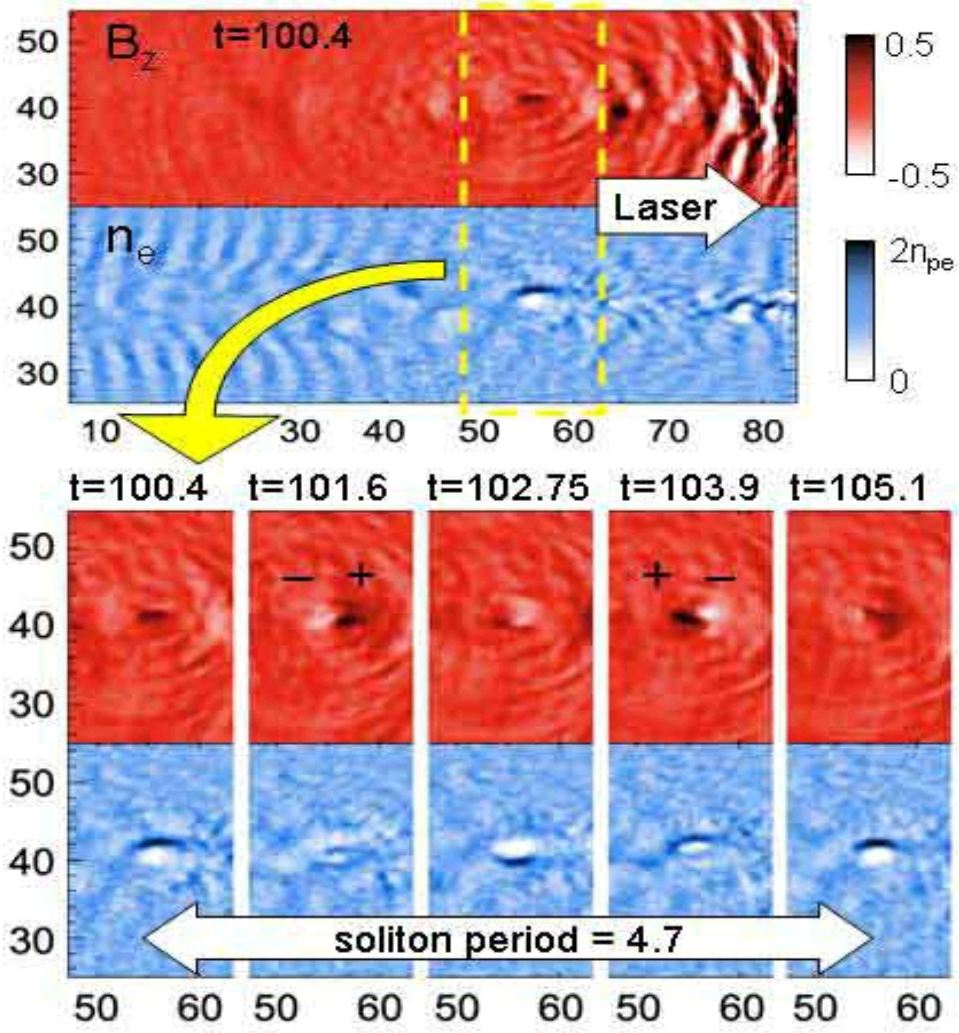

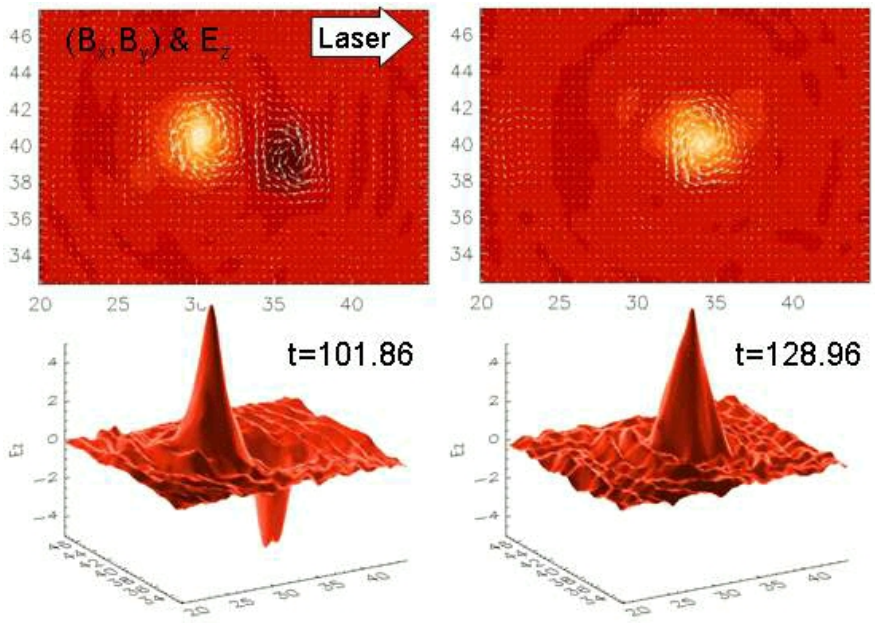

Merging of two S-solitons behind the short laser pulse in PIC simulation. In the upper row the white arrows represent the magnetic field in the plane, the background colour scale represents the electric field perpendicular to the plane. In the bottom row Ez component is shown. Pulse: a=eE/(me omega c)=3, S-polarized, omega_pe/omega =0.3

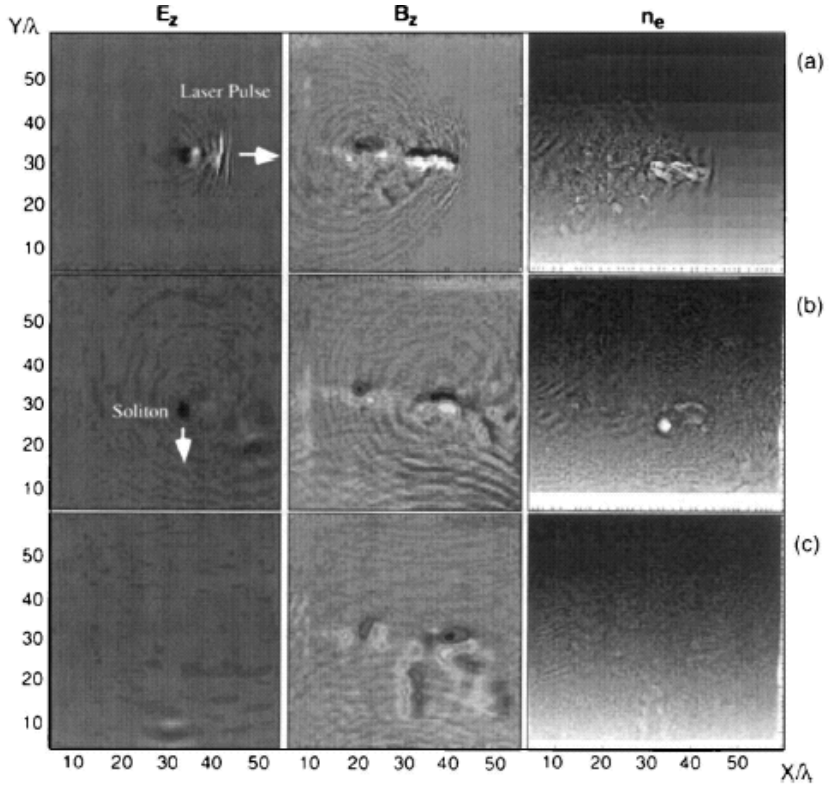

soliton drifting in an inhomogeneous plasma

3D solitons

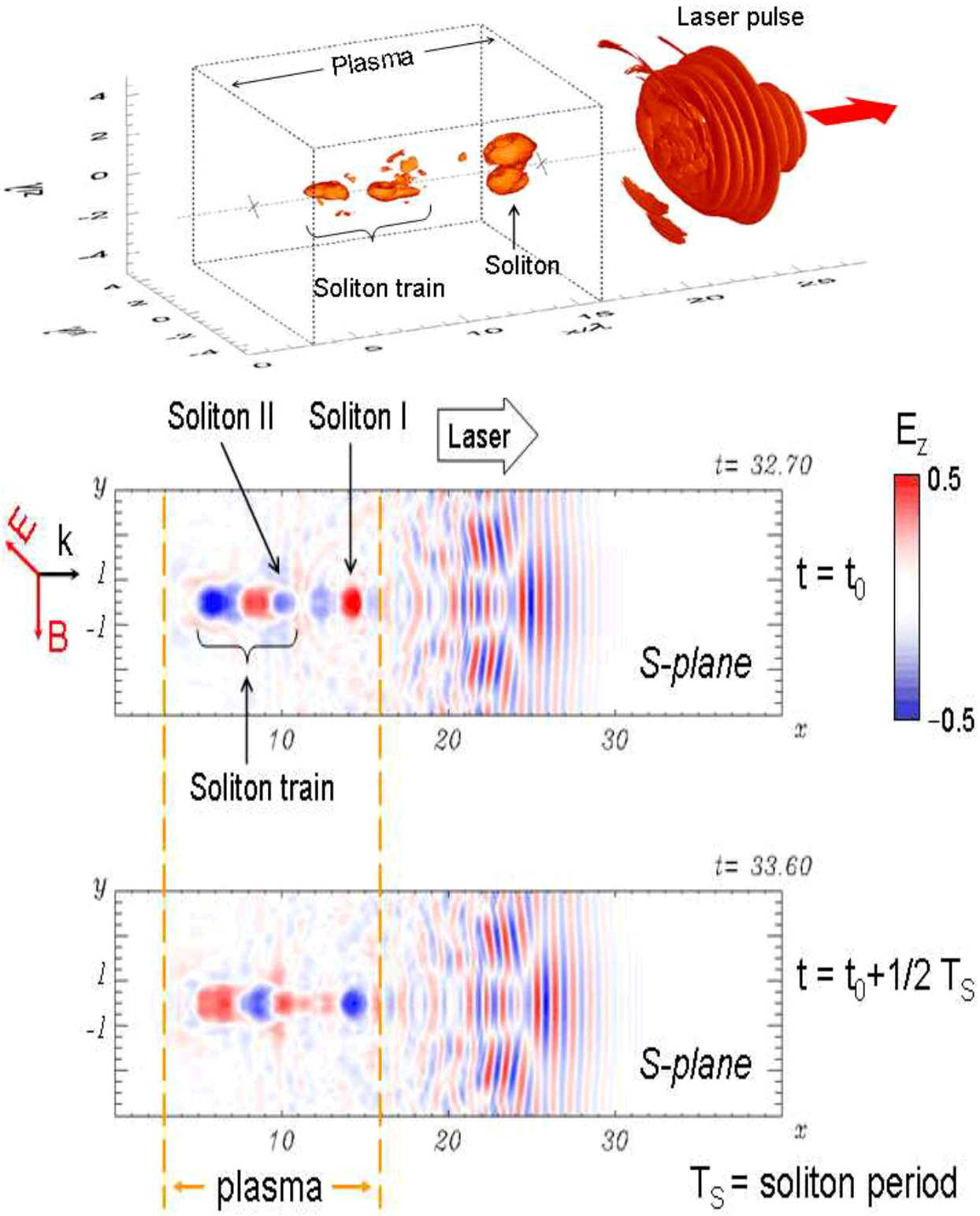
Laser pulse
Plasma
Soliton train
Soliton
Soliton II
Soliton I
Laser
E
k
B
t= 32.70
t = t0
S-plane
Soliton train
Ez
0.5
-0.5
t= 33.60
t = t0+1/2 TS
S-plane
plasma
TS = soliton period

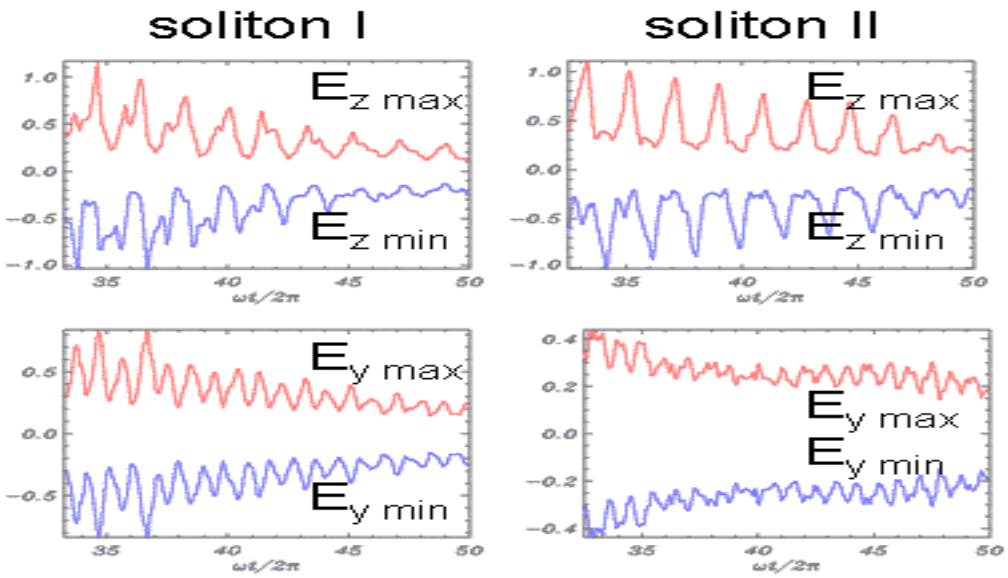
soliton I
soliton II
$E_{z\,max}$
$E_{z\,min}$
$E_{y\,max}$
$E_{y\,min}$
ωt/2π

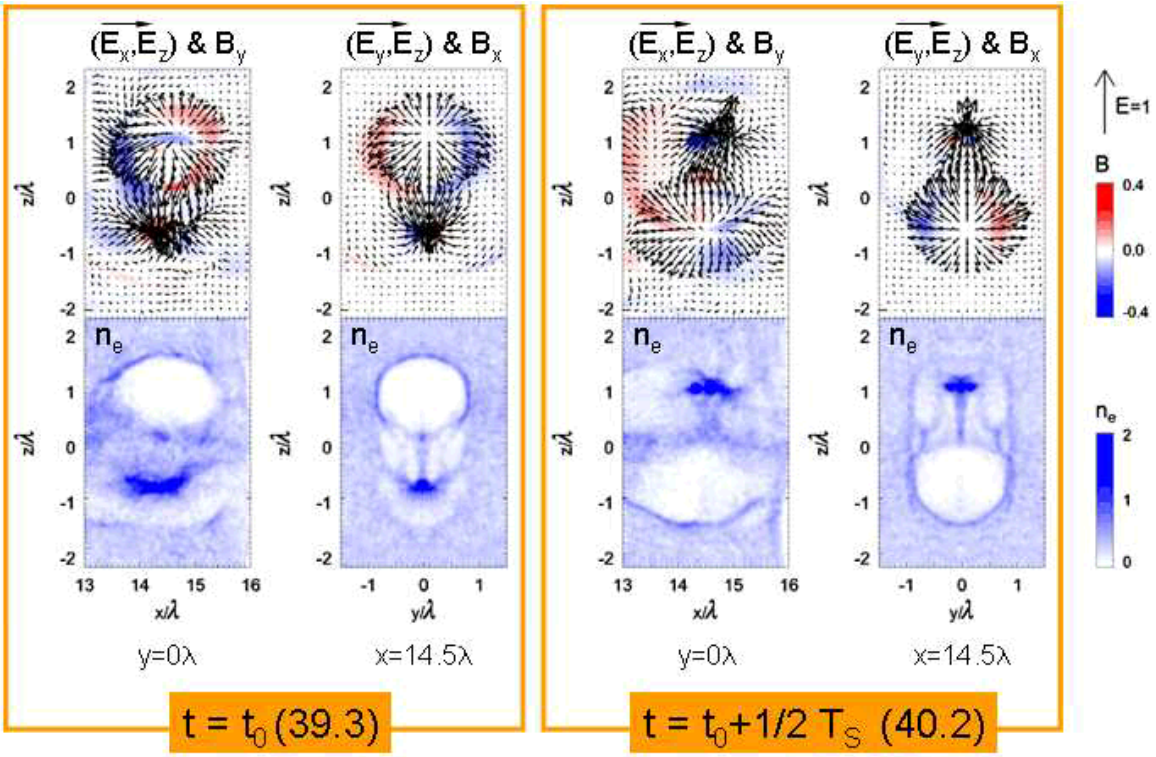
$(\vec{E}_x,\vec{E}_z)$ & B_y
$(\vec{E}_y,\vec{E}_z)$ & B_x
n_e
z/λ
x/λ
y/λ
y=0λ
x=14.5λ
t = t_0 (39.3)
t = t_0+1/2 T_S (40.2)
E=1
B
n_e

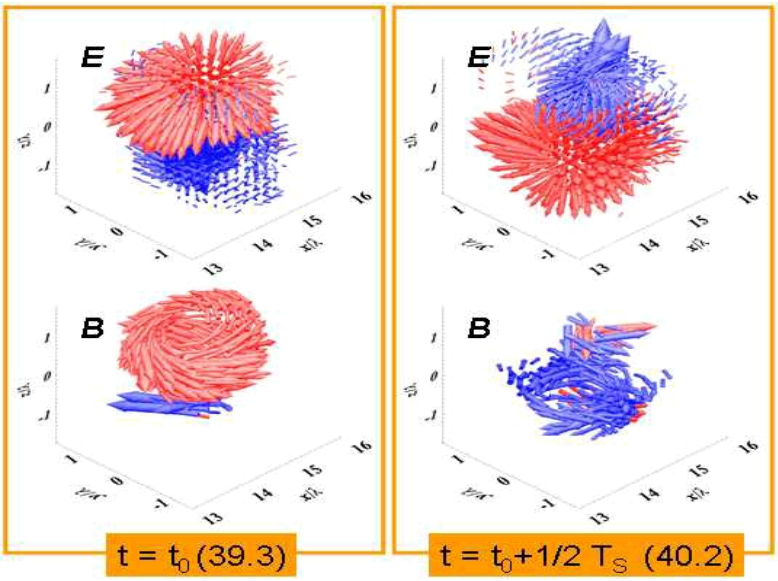
E
B
t = t0 (39.3)
E
B
t = t0+1/2 TS (40.2)

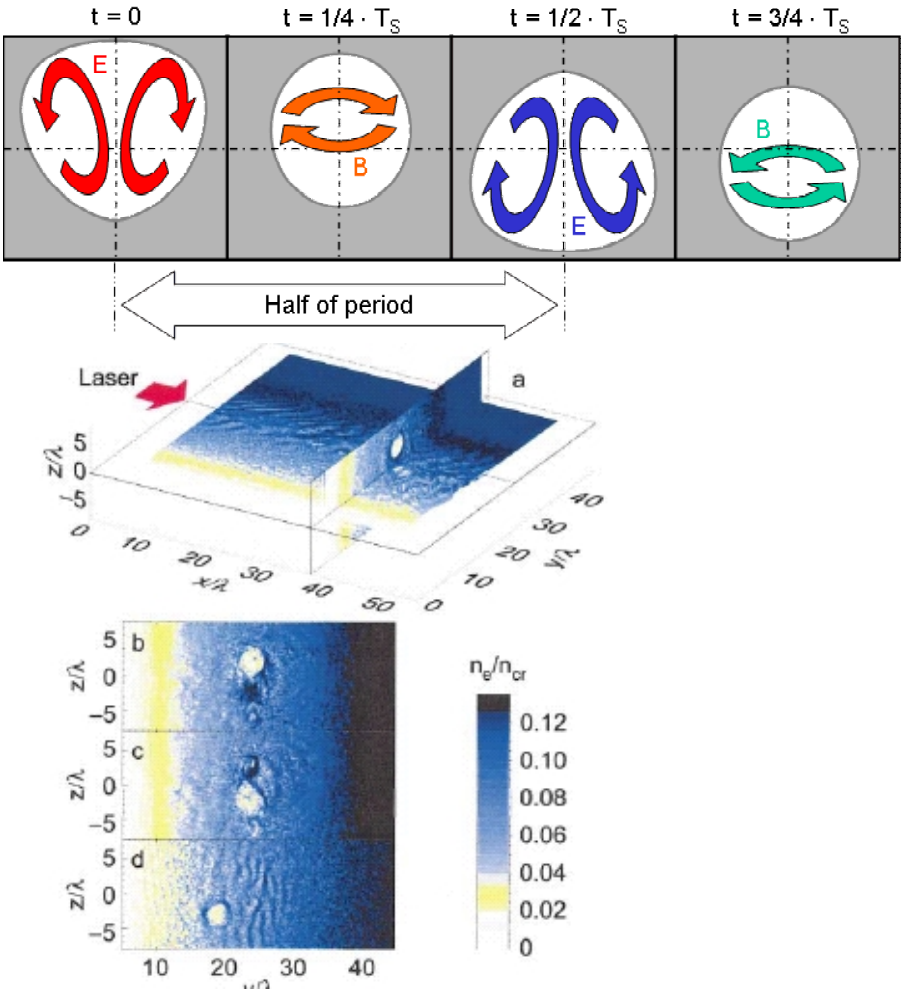
t = 0
t = 1/4 · TS
t = 1/2 · TS
t = 3/4 · TS
E
B
B
E
Half of period
Laser
a
b
c
d
ne/ncr
0.12
0.10
0.08
0.06
0.04
0.02
0

postsolitons

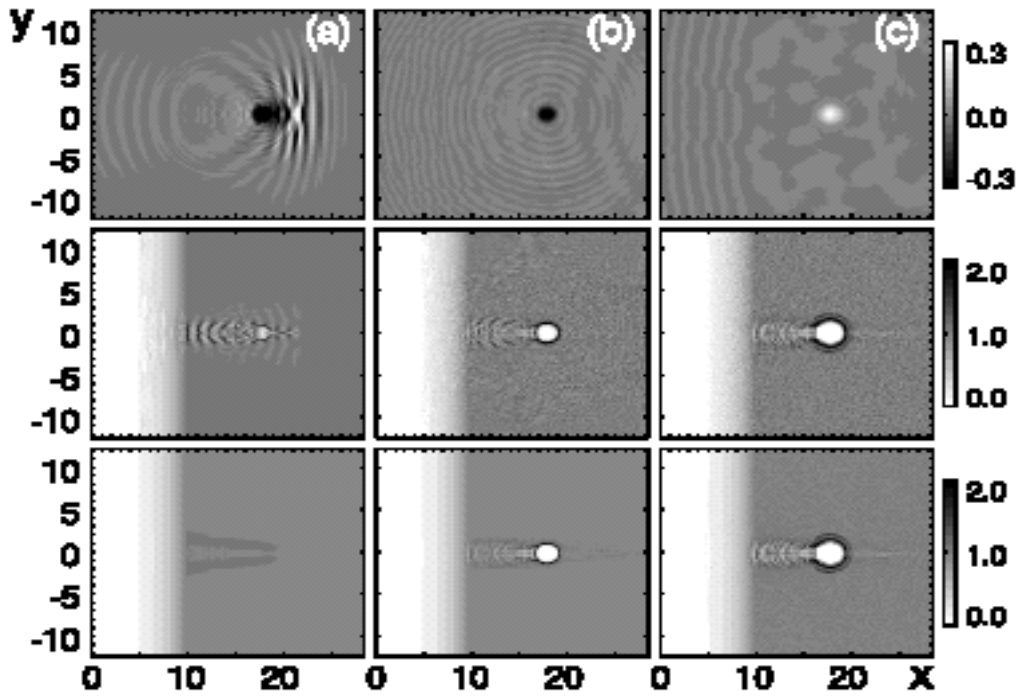

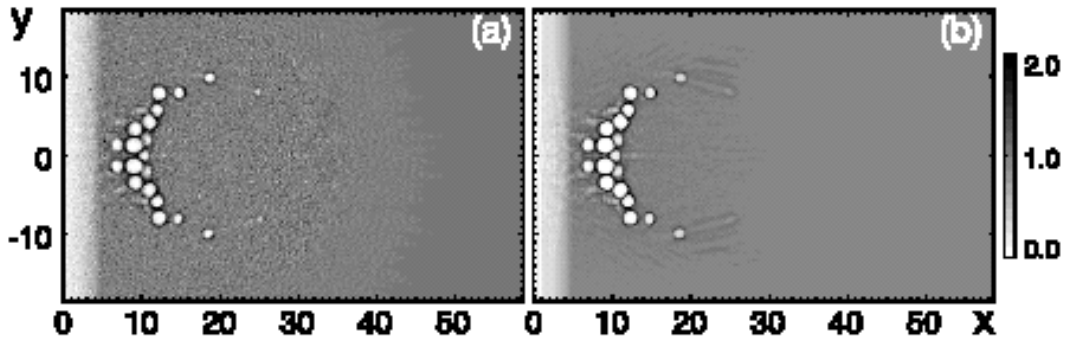

proton imaging